ACS APPLIED MATERIALS & INTERFACES

Research Article

www.acsami.org

Molecular-Scale Understanding of Cohesion and Fracture in P3HT:Fullerene Blends

Naga Rajesh Tummala,[†] Christopher Bruner,[‡] Chad Risko,*[,†,§] Jean-Luc Brédas,*[,†,∥] and Reinhold H. Dauskardt*[,‡]

[†]School of Chemistry and Biochemistry & Center for Organic Photonics and Electronics, Georgia Institute of Technology, Atlanta, Georgia 30332-0400, United States

[‡]Department of Materials Science and Engineering, Stanford University, Palo Alto, California 94305-4034, United States

[§]Department of Chemistry & Center for Applied Energy Research (CAER), University of Kentucky, Lexington, Kentucky 40506-0055, United States

[∥]Solar & Photovoltaics Engineering Research Center, King Abdullah University of Science and Technology, Thuwal 23955-6900, Kingdom of Saudi Arabia

Supporting Information

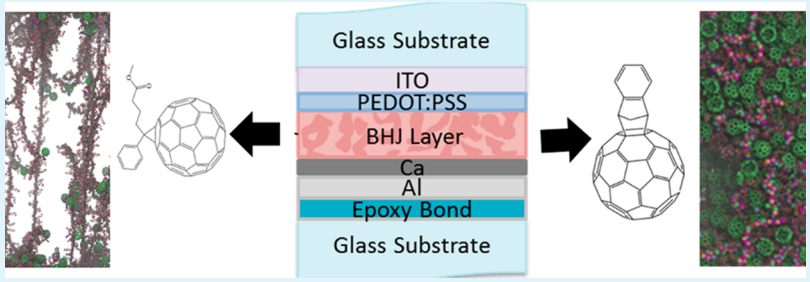

ABSTRACT: Quantifying cohesion and understanding fracture phenomena in thin-film electronic devices are necessary for improved materials design and processing criteria. For organic photovoltaics (OPVs), the cohesion of the photoactive layer portends its mechanical flexibility, reliability, and lifetime. Here, the molecular mechanism for the initiation of cohesive failure in bulk heterojunction (BHJ) OPV active layers derived from the semiconducting polymer poly(3-hexylthiophene) [P3HT] and two monosubstituted fullerenes is examined experimentally and through molecular-dynamics simulations. The results detail how, under identical conditions, cohesion significantly changes due to minor variations in the fullerene adduct functionality, an important materials consideration that needs to be taken into account across fields where soluble fullerene derivatives are used.

KEYWORDS: *cohesion and fracture, P3HT, substituted fullerenes, solar cells, thin films, molecular dynamics*

INTRODUCTION

To establish bulk heterojunction (BHJ) organic photovoltaics (OPV) as a commercially viable technology requires development of solution-processing protocols that can lead to large-scale, cost-effective manufacturing (e.g., roll-to-roll printing) and to ensure mechanical reliability and flexibility. The current OPV literature remains predominantly concerned with the design of new molecules and polymers with well-defined electronic, optical, and redox properties as well as investigations of the intrinsic electronic processes underlying photocurrent generation. Although there is increasing interest in the mechanical properties of BHJ active layers,[1−9] and such studies are common for traditional polymers,[10,11] the efforts in the OPV arena remain limited when compared to performance efficiency studies.[12−16]

Along with the electronic processes involved in photocurrent generation, the active-layer mechanical properties inherently depend on the multiphase morphology of the BHJ thin films[17−22] and therefore are contingent on the thin-film processing protocols and the nature and strength of non-covalent, solid-state intermolecular interactions. However, a molecular-scale understanding of these properties, which is key to the design of more mechanically and electronically robust active layers, remains elusive. Hence, studies that detail these relationships in BHJ OPV—and, in general, across the field of organic electronics—are critical as they provide information concerning the energetic implications of the events that induce mechanical strain in the environment where the devices will be implemented.

Electron-acceptor materials derived from fullerenes—and in particular the phenyl butyric acid methyl ester substituted C_{60} and C_{70} derivatives ($PC_{61}BM$ and $PC_{71}BM$, respectively)—among a multitude of others[23−26] continue to dominate the BHJ OPV literature. However, it is not clear how the chemical

Received: March 12, 2015
Accepted: April 21, 2015
Published: April 21, 2015

DOI: 10.1021/acsami.5b02202
ACS Appl. Mater. Interfaces 2015, 7, 9957−9964

substitution patterns of the solubilizing groups influence the electronic and mechanical properties of these composite materials, as there remain many intricate details that need to be unfurled at the molecular- and nanoscales. Notably, fullerenes have been exploited in other composite blends;[27−32] however, their traction in these applications remains limited due to restrictions in terms of solubility, processability, and the resulting materials properties.[27] Hence, there is a wide-ranging need to understand these molecular materials and how subtle variations in chemical structure can impact material performance.

Here, we present a combined experimental and theoretical study that reveals how seemingly modest changes in the solubilizing adducts of fullerenes, which have found wide use in OPV and across many other electronics applications, and polymer molecular weight impact the cohesive properties of pure and blend thin films. In particular, four-point bend (FPB) experiments and molecular dynamics (MD) simulations are combined to evaluate the cohesion and stress−strain behavior of two amorphous fullerene derivatives, namely, phenyl-C_{61}-butyric acid methyl ester (PCBM) and the indene-C_{60}-mono adduct (ICMA), and poly(3-alkylthiophene) [P3HT]:fullerene mixtures. The theoretical results directly correlate with the experimental measurements of adhesion/cohesion and reveal how small changes in chemistry, i.e., the nature of the substituent appended to the fullerene, and polymer entanglements dependent on the P3HT molecular weight can control the cohesive properties of these films. Hence, the results we obtain provide an important molecular-scale insight that can be used in materials and process design, a critical feature to increase production yields, of these electronically active materials.

An implicit assumption in this work is that the weakest links within the active layer are located at either the polymer:-fullerene interface or within amorphous mixed regions. While many factors contribute to film cohesion, including para-crystallinity,[2] crystal domain sizes,[4] and postdeposition processing protocols (e.g., annealing[33,34]), the connection among these factors is not well understood and is outside the scope of the present manuscript. As we show below, the cohesion is dependent on the chemical nature of the polymer and fullerene, and hence we expect that different blend systems, processed via different means, can present marked differences in mechanical properties.

METHODOLOGY

OPV Device Preparation. All OPV devices were prepared by spin-casting the BHJ layer (consisting of ICMA (Plextronics), PCBM (Solenne), and P3HT (Rieke Metals) or blends thereof) onto 30 nm of poly(3,4-ethylenedioxythiophene):poly(styrenesulfonate) (PEDOT:PSS) deposited on indium tin oxide (ITO, 120 nm) glass substrates, as previously described.[1,33]All active layers were cast from chlorobenzene solutions that were allowed to stir at 65 °C overnight (90 °C for ICMA in chlorobenzene). The cast films were then allowed to dry for 12 h. Ca and Al metal electrodes were deposited in a thermal evaporator on top of the active layer.

Adhesion/Cohesion Testing. All OPV devices used for cohesion testing were processed into four-point bend (FPB) test specimens, as previously described.[3] The FPB specimens were compressed under displacement control with a displacement rate of 0.25 μm/s and a moment arm, L, of 6.5 mm in a high resolution micromechanical testing system (DTS, Menlo Park, CA, USA). From the load versus displacement curves, the critical load, P_c, was extracted and used to calculate the cohesion energy, G_c, using the following equation:[1,5]

$$G_c = \frac{21P_c^2L^2}{16b^2h^3E'} \quad (1)$$

where E' is the plane strain modulus and b and h are the specimen width and half-height, respectively. Methodology and results for surface analysis are reported in the SI.

Molecular Dynamics (MD) Simulations. MD simulations of P3HT oligomers and P3HT:fullerene mixtures, owing to the compatibility of in-house scripts to generate oligomers of different sizes, were carried out with the large-scale atomic/molecular massively parallel simulator (LAMMPS)[35] and simulations of pure fullerenes are performed in the GROMACS[36,37] software suite. A Nose-Hoover thermostat was used to keep the temperature constant during the simulations with a relaxation time constant of 100 fs. Internal pressure was maintained as implemented in the Parinello−Rahman barostat (in GROMACS)[38−40] and Nosé−Hoover barostat (in LAMMPS) with the damping parameter set to 500 fs. Atomic coordinates were stored at 20−50 ps intervals depending on the system size; the thermodynamic parameters (bond, angle, dihedral, van der Waals energy, electrostatic interactions) were stored every 0.5 ps. The results reported here are computed from averages of the final 2−5 ns of the simulations.

The OPLS-AA (optimized potentials for liquid simulations—all atom) force-field[41] parameters were used for PCBM and ICMA; previous work[24,42,43] has shown these force-field parameters accurately describe the intermolecular interactions for PCBM.[24] For simulations of the pure fullerene derivatives, 400 molecules were randomly placed in the box and simulated at 1000 K for at least 2 ns. The resulting amorphous structures were then equilibrated at 300 K for at least 10 ns. The final structure was replicated twice along the z-dimension, such that the number of molecules in the simulation box was at minimum 800. This final configuration was simulated at elevated temperature and pressure (1000 K and 5 bar) and equilibrated at 300 K and 1 bar. Care was taken to make sure the resulting final configuration is equilibrated and free from simulation artifacts. Miscibility parameters (i.e., Hildebrand parameters) and surface energies for the fullerenes were computed as previously described.[24]

P3HT was modeled using modified OPLS-AA parameters.[44,45] Simulations of P3HT:fullerene mixtures were carried out with 50-monomer P3HT chain lengths (8.32 kDa) at P3HT weight-percents of 25% (11 P3HT oligomers and either 328 ICMA or 302 PCBM), 50% (23 P3HT oligomers and either 229 ICMA or 210 PCBM molecules), and 75% (34 P3HT oligomers and either 117 ICMA or 104 PCBM molecules). P3HT/fullerene bilayer simulations using the same 50-monomer P3HT model were carried out with 48 P3HT oligomers and 400 fullerenes. Blend simulations using 200-monomer P3HT oligomers, with 25 P3HT molecules and 1021 ICMA or 920 PCBM molecules (50% P3HT weight fraction) were carried out to show differences in material behavior at the onset of entanglement (P3HT oligomer length = 50) and where entanglements are $\gg$1 (P3HT oligomer length = 200). P3HT oligomers and fullerenes were randomly placed in simulation boxes at densities less than 0.3 g/cm^3, and soft potentials as available in LAMMPS were used to minimize molecular overlap. Energy minimization followed, and MD simulations were performed at 550 K in *NVT* ensembles for at least 2 ns. Further simulations were performed in *NPT* ensembles at 550 K and 1 atm, followed by runs at 300 K and 1 atm. Total simulation times for 50-monomer P3HT mixtures were run for 50 ns or more, and at least 25 ns simulations were run for 200-monomer P3HT mixtures. Equilibrium conditions were validated through structural characterization of two 300 K simulations that were started from different points, separated by at least 5 ns, within the 550 K simulations. Simulation protocols for pure P3HT oligomers were recently reported.[46]

To examine the modulus in both pure and blend films, a series of MD simulations with incremental strain of 0.005 ($\Delta L/L$) were performed for 100−200 ps. The z component of the stress tensor was selected to compute the uniaxial elongation (tensile) modulus. The slope of the stress vs strain plot in the linear regime (less than 5% strain) is reported as the modulus. To determine the critical fracture

DOI: 10.1021/acsami.5b02202
ACS Appl. Mater. Interfaces 2015, 7, 9957−9964

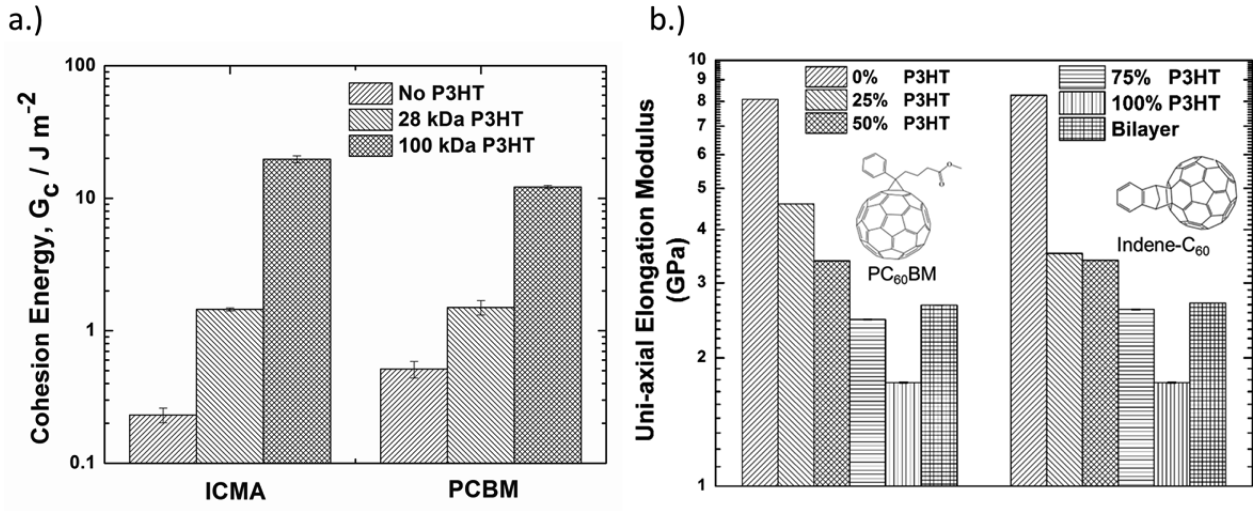

Figure 1. (a) BHJ OPV cohesion energy (with mechanical failure occurring within the active layer), plotted on a logarithmic scale, as determined via four-point bend (FPB) experiments. All blends consisted of a 1:1 polymer:fullerene mass ratio. The fracture energy for P3HT(100 kDa):PCBM is reproduced from previous work.[3] (b) Uniaxial elongation/tensile moduli derived from MD simulations with P3HT chain lengths of 50 monomers.

energy (G_c), simulations were performed, starting from equilibrated configurations, with constant strain (elongation) rate (1 pm/ps) using the SLLOD[47] equations of motion coupled to Nose−Hoover thermostat as implemented in LAMMPS. Typically, the energy of the system decreases as the box dimension increases along the dimension of pulling; however, when the energy lost is equivalent to G_c, an increase in energy is observed before convergence (due to the evolution of two surfaces with a vacuum gap between them). The difference in energy (sum of the van der Waals and electrostatic terms) between the bulk system and the point at which the direction of energy change reverses divided by the surface area (here, the cross section area of the simulation box) yields critical fracture energy (Figure S3). These calculations were repeated at minimum three times and the standard deviation is reported as error bars in Table S2. To understand the stress−strain behavior of the polymer:fullerene-derivative mixtures, for both BHJ blends and bilayers, and to compare with the pure polymer systems, simulations were performed where the simulation box was elongated in the z-dimension with constant strain rate with SLLOD[47] equations of motion coupled to the Nose−Hoover thermostat as implemented in LAMMPS. Since the surfaces after fracture in the case of polymers are not smooth, the G_c values for polymer systems cannot be evaluated with a procedure similar to that used for fullerenes. The average numbers of entanglements $\langle Z \rangle$ were determined using the primitive path analysis with the Z1 software.[48−51]

RESULTS AND DISCUSSION

Starting with pristine fullerene films (in full device configurations), the four-point bend experiments (Figure S1) reveal that the fracture energy (Figure 1) of ICMA (0.23 ± 0.03 J m^{-2}) is twice as small as that for PCBM (0.51 ± 0.07 J m^{-2}). This is a somewhat surprising result considering that the majority of the molecular material in each instance is comprised of the same C_{60} fullerene cage. These data suggests that the substituent chemistry plays an important role in cohesion (vide infra). These chemical differences are also partly evidenced by the fact that ICMA possesses a lower degree of solubility in chlorobenzene as compared to PCBM, which results in only partially uniform ICMA films (with scattered fullerene aggregates), as opposed to the smooth, completely uniform films of PCBM. Importantly, such ICMA aggregates could act as defects that increase localized stress within the film, reducing the film cohesion energies.

Turning to P3HT:fullerene BHJ devices, active layer films that incorporate 28 kDa P3HT in a 1:1 polymer:fullerene mass ratio show an increase in the cohesion energy compared to the pure fullerene films, with both blends (1.45 ± 0.04 J m^{-2} for P3HT:ICMA and 1.50 ± 0.19 J m^{-2} for P3HT:PCBM) having similar cohesion energies, a result contrary to previous findings.[1] Importantly, the cohesion energy increases to 12.2 ± 0.3 J m^{-2} for PCBM:P3HT blends when the P3HT M_W is increased to 100 kDa; at this molecular weight, the P3HT chain is approximately 600 monomers long and the P3HT:PCBM BHJ layer thickness is 99 ± 2 nm. MD simulations point to such a 600-monomer length to be roughly equal to 10−12 times the entanglement length (N_e);[46] thus, a significant degree of interchain entanglements is expected.

P3HT:ICMA devices made with 100 kDa P3HT (here, the BHJ layer thickness is slightly larger at 112 ± 3 nm) have a cohesion energy of 19.7 ± 1.2 J m^{-2}. While some of the increased cohesion of this blend may be attributed to the slightly greater film thickness when compared to P3HT:PCBM, previous work has shown that a P3HT:PCBM BHJ film made with 100 kDa P3HT and a film thickness of 174 nm results in a smaller cohesion energy of 16.5 ± 1.3 J m^{-2} vs this thinner P3HT:ICMA film. Taken together, these results underline features in the modified chemistry of the fullerenes and their subsequent interactions with P3HT as one of the sources for the differences in cohesion energies.

We now turn to results from MD simulations to examine the differences in the fracture properties of the bulk fullerenes and polymer:fullerene mixtures at the molecular scale. We begin with a focus on the bulk packing and energetic properties of the pure (amorphous) materials. For the two fullerene derivatives, the radial distribution functions (RDFs, determined from the fullerene centers-of-mass) derived from the MD simulations (see the Supporting Information, SI, Figure S2) indicate that ICMA has more first-shell contacts when compared to PCBM, though there is little variation in the position and magnitude of the first RDF peak (at 1.0 nm) when comparing the two fullerenes. There do exist some differences, however, in the second molecular shell and beyond (at distances greater than 1.25 nm), e.g., ICMA has a larger degree of coordination, and these longer-range differences do lead to variances in bulk

DOI: 10.1021/acsami.5b02202
ACS Appl. Mater. Interfaces 2015, 7, 9957−9964

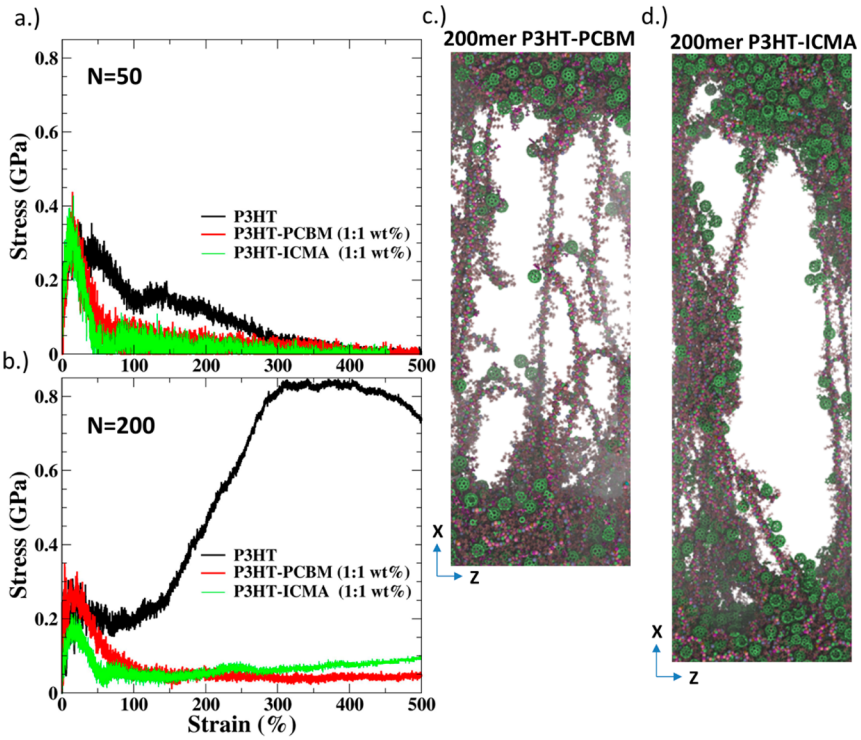

Figure 2. Simulated stress (GPa) vs strain (%) for P3HT and P3HT:fullerene mixtures incorporating different P3HT chain lengths. (a) P3HT of chain length 50, (b) P3HT of chain length 200, (c and d) Representative simulation snapshots of 200-mer P3HT:PCBM and P3HT:ICMA mixtures at ≈300% strain, respectively. The initial box lengths along *x*- and *z*- are 17.7 and 7.5 nm, respectively, for P3HT:PCBM and 13.6 and 12.6 nm, respectively, for P3HT:ICMA.

packing and mechanical properties. The presence of the larger adduct in PCBM leads to a slightly smaller equilibrated density (by 0.03 g/cm^3) as compared with the nonpolar ICMA, a feature of importance in terms of the impact on the mechanical and cohesive properties.

The calculated Hildebrand parameters for PCBM (10.7 [cal/cm^3]$^{1/2}$, as previously reported[24]), ICMA (10.0 [cal/cm^3]$^{1/2}$), and P3HT (9.2 [cal/cm^3]$^{1/2}$) compare very favorably with experimental data (see Supporting Information, Table S2).[52,53] Decomposition of the total interaction energy into dispersive, electrostatic, and hydrogen-bonded interactions yields the Hansen miscibility parameters (Table S2).[54] Though the dispersion parameters[54] (δ_D) are identical for the two fullerenes (9.8 and 9.9 [cal/cm^3]$^{1/2}$ for ICMA and PCBM, respectively), the contribution from electrostatic interactions is reduced in ICMA when compared with PCBM, as the combined hydrogen-bond plus electrostatic term (δ_P + δ_H) is 4.0 (cal/cm^3)$^{1/2}$ in PCBM and only 2.0 (cal/cm^3)$^{1/2}$ in ICMA; the same term in P3HT is 3.0 (cal/cm^3)$^{1/2}$. The Hansen parameters[54,55] arising from the simulations suggest that the larger (δ_P + δ_H) term in PCBM (coming from the polar side-chain) will lead to a smaller driving force for mixing with P3HT when compared to ICMA, even though both fullerene derivatives lie within the solubility sphere of P3HT.[56] This result is consistent with the experimental observation of the formation of fullerene clusters in P3HT:PCBM mixtures[57,58] and the improved miscibility of P3HT:indene-C_{60}-bis-adduct (ICBA) blends when compared to P3HT:PCBM.[58]

When considering the mechanical properties of the pure materials, the calculated uniaxial elongation/tensile moduli for the substituted fullerenes are determined to be 8.1 ± 0.01 GPa for PCBM and 8.3 ± 0.01 GPa for ICMA. While the differences in tensile modulus might at first appear to be minor, the extremely small error bars reveal that this is a notable difference. The 0.2 GPa increase in modulus for ICMA vs PCBM is a function of the shorter adducts, which, as discussed earlier in terms of the RDF's, results in closer packing and higher density. For comparison, MD simulations of amorphous, bulk C_{60} result in an elongation modulus of 9.6 ± 0.3 GPa, in general agreement with experiment, though we note these simulations were performed in a smaller simulation box (containing 400 C_{60} molecules) than our other simulations and resulted in slightly larger error bars; the experimentally determined modulus of C_{60} is 10 to 20 GPa[59−61] and is strongly dependent on the crystallinity of the sample and the direction of elongation.[61]

The theoretically determined cohesion energy, obtained from deformation simulations described in the ESI, for ICMA is 0.36 ± 0.05 J m^{-2}, a result somewhat larger than the experimentally measured value of 0.23 J m^{-2}. As noted above, the ICMA clusters formed during film formation from deposition with chlorobenzene could reduce the film cohesion.[62] On the other hand, the calculated cohesion energy for PCBM is 0.50 ± 0.05 J m^{-2}, a result in very close agreement with experiment.

Thus, the larger modulus of ICMA does not necessarily translate into stronger cohesion, as the cohesion energy is also dependent on long-range interactions. As described by the Griffith fracture criteria,[63] the critical cohesion energy (G_c) of a brittle material is generally twice the surface energy. For both fullerene derivatives, the G_c value evaluated from the simulations is approximately five times as large as the surface energy; hence, the larger fracture energy for PCBM could be a result of its larger surface energy (0.1 J m^{-2}) compared to ICMA (0.055 J m^{-2}). These values should be treated as upper

DOI: 10.1021/acsami.5b02202
ACS Appl. Mater. Interfaces 2015, 7, 9957−9964

bounds with respect to experiment,[64,65] as the long-range electrostatic interactions are not taken into consideration when calculating these values. The larger surface energy for PCBM arises from the polar butyric methyl ester tail on the PCBM that provides intermolecular C−H−O hydrogen bonding, resulting in the formation of supramolecular assemblies[66] that may contribute to the larger cohesion energies.

MD simulations with different M_w P3HT[46] reveal that the entanglement length (N_e) of P3HT is 50−60 monomer units (corresponding to an entanglement molecular weight, M_e, of 10 kDa). It is useful to point out that a $M_w > 4M_e$ ($N/N_e > 4$) is required to observe an increase in cohesion energies within polymer films.[67] Within the linear elastic regime (engineered strain less than 5%), the uniaxial elongation modulus is directly related to the fullerene weight-percent in the system (Figure 1). The calculated uniaxial modulus of pure P3HT converges to 1.6 ± 0.1 GPa when simulated with 50 or 100 monomers,[46] indicating that the moduli of the fullerene derivatives are approximately five times larger than that of P3HT, in agreement with experiment.[68] Within polymer:fullerene composites, the modulus increases with increasing fullerene weight fraction. The increase in the uniaxial modulus is, however, nonlinear. It is interesting that, for the three simulated weight fractions (25, 50, and 75%), minor differences in modulus are observed when comparing the different fullerene derivatives. As discussed earlier, for low M_w P3HT, P3HT:PCBM has a marginally larger cohesion energy and also a larger uniaxial elongation modulus when compared to P3HT:ICMA, a result that may be attributed to the smaller cohesion energy for ICMA. These differences are significant in the sense that even within 5% strain, the changes due to interactions between P3HT and the fullerene derivatives are rather evident, even for the 50-monomer P3HT. It is expected that the differences will be larger for higher M_w chains. The change in the polymer physical characteristics upon mechanical strain when mixed with fullerene derivatives could answer fundamental questions for differences in cohesion/fracture in BHJ devices.

Stress vs strain curves for pure P3HT and 1:1 weight-percent (wt %) mixtures of P3HT:PCBM and P3HT:ICMA for 50-monomer (8.3 kDa) and 200-monomer (33.2 kDa) P3HT chain lengths are shown in Figure 2. As expected, the stress for 50-monomer P3HT initially increases with strain and then decreases. Between 100 to 200% strain, the stress plateaus at 0.15 GPa before finally falling to zero, which is typical of polymer networks with entanglements.[69] However, the addition of fullerene derivatives to P3HT results in no plateau with strain. Simulations with different P3HT:fullerene ratios (as compared to the 1:1 wt % ratio discussed here) show similar behavior, indicating that the system may not undergo craze formation but, instead, the crack will simply propagate along the plane of least resistance,[69] e.g., along a particular P3HT/fullerene interface. When the P3HT polymer chain length is increased to 200 monomers, a plateau of 0.2 GPa is observed at 100% strain for the pure polymer. As the stress continues to increase, a second plateau is reached at strains of 150% to 250%. This feature is indicative of significant entanglements that resist fracture. This behavior is expected when the number of entanglements is ≫1 and the polymer chain length is at least greater than twice N_e (depending on the nature of the polymer backbone). In contrast to P3HT:fullerene blends with 50-monomer P3HT, 200-monomer P3HT:fullerene blends do show a plateau past 100% strain. For ICMA:P3HT mixtures, a slightly larger stress is observed at strains greater than 200%. This result is indicative of a greater degree of entanglements in this blend compared to the P3HT:PCBM mixtures, although N_e is smaller than those in pure P3HT. Representative snapshots (see Figure 2) indicate that upon elongation, due to larger intermolecular interactions, P3HT:ICMA mixtures form a thick intermixed fibrillar structure in contrast to the independent P3HT fibrils with fewer bound PCBM molecules in the case of P3HT:PCBM mixtures. These differences illustrate that the fracture along P3HT:PCBM interfaces occurs at lower stress than that in P3HT:ICMA.

Simulations of polymer/fullerene bilayers were conducted to provide insight on whether fracture can occur at interfaces between pure domains. The simulations were initiated with defined boundaries at the bilayer interface (before any intermixing at the interface may occur, see Figure S4). In brief, perfect interfaces were simulated in an *NPT* ensemble for 1 ns at 550 K and, at minimum, 10 ns at 300 K; no significant changes were observed in the final 5 ns. Density profiles (shown in Figure S4) from the simulations point to the fact that P3HT protrudes into and mixes with the ICMA phase more than it mixes with the PCBM phase. When subjected to uniaxial elongation at a strain rate of 1 nm/ns in the direction perpendicular to the bilayer, the fracture occurs within the ICMA layer for the P3HT/ICMA bilayer (mainly due to the weaker cohesion within ICMA than at the P3HT/ICMA interface, see Figure 3), whereas the fracture occurs at the

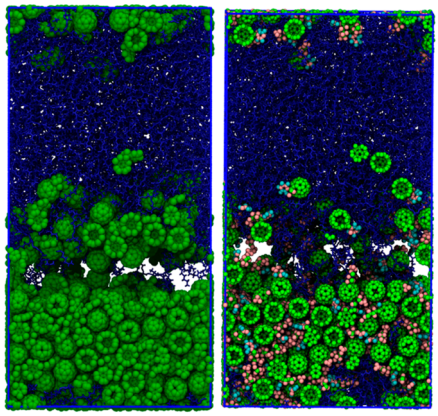

Figure 3. Representative simulation snapshots of a bilayer comprised of P3HT (50-monomer chain length) with ICMA (left) and PCBM (right). Fracture occurs when the simulation box is deformed along the plane of the page.

interface for P3HT/PCBM bilayer. It is useful to emphasize that the cross-section area of the simulation box is 8.5 nm × 8.5 nm and is therefore of comparable scale to film voids occurring during the fracture. That there are differences where fracture takes place in the bilayer system, points to the reason for the slightly smaller cohesion energy of the P3HT:ICMA blend with low M_w P3HT compared to P3HT:PCBM. However, no significant difference in the stress−strain curves for the bilayer systems were observed, which can be a reflection of the fact that the simulations were performed only for 50-monomer P3HT.

Finally, the change in stress within polymer:fullerene mixtures has been quantified by computing the average number of polymer entanglements within the mixtures. For polymer:-fullerene mixtures with 50-monomer P3HT, there is a linear

DOI: 10.1021/acsami.5b02202
ACS Appl. Mater. Interfaces 2015, 7, 9957−9964

decrease in the average number of entanglements $\langle Z \rangle$ with increasing fullerene content for both fullerene systems using primitive path analysis (see Figure S5 in the ESI).[48] The entanglement differences among 1:1 mixtures of P3HT:fullerene derivatives for 50-monomer P3HT are within the simulation statistical noise. However, the differences become significant when 200-monomer P3HT is used in the polymer:-fullerene mixtures, indicating that attractive P3HT-ICMA interactions would allow P3HT to kink and coil more in the presence of ICMA compared to PCBM. Note that the average number of entanglements decreases from 5.0 for ICMA:P3HT mixtures to 4.0 for PCBM:P3HT mixtures, indicating a larger N_e value for P3HT in the presence of PCBM. This suggests that decohesion will readily occur within the weaker fullerene phase or at the interface, and allow for propagation into the polymer matrix. Effectively, the fullerenes act as defects within the polymer matrix and, during decohesion, may allow for cavitation, resulting in the polymer phase pulling away from the fullerenes.[70] This suggests that the nature of the polymer is what principally affects BHJ layer cohesion.

The significant differences in cohesion energy between high M_w P3HT:PCBM and P3HT:ICMA may be partly attributed to the increase in kinks and entanglements in P3HT:ICMA. It must be noted that the P3HTs used in the FPB experiments possessed dispersities of 2, with a regioregularity of about 92%. This reduced regioregularity can lead to smaller N_e and a greater degree of entanglements, which would increase the fracture energy. For smaller chain lengths, the fullerenes still affect the polymer properties, though the increased polymer rigidity minimizes these effects. However, when the polymer chain lengths permit semiflexibility (where $N \gg N_e$), mixing fullerenes or nanoparticles to the polymers greatly influences the degree of polymer chain entanglements.

CONCLUSIONS

From our combined experimental and theoretical study, we propose that the primary mechanism of failure during fracture in P3HT:fullerene BHJ films under tension occurs as the polymer pulls away from the fullerene interface, which results in void formation. As strain increases, voids grow in the polymer layer and attempt to join. For low-M_w polymers ($N < 4N_e$), the polymer chains are able to slide past each other smoothly, resulting in small fracture energies. However, for high-M_w polymers ($N > 4N_e$), polymer chain entanglement resists mechanical loading, resulting in plastic deformation within the BHJ layer. Although P3HT is the work horse for various fundamental studies involving OPV, similar studies for the donor−acceptor conjugated polymers that are increasingly used in OPV are essential for understanding in-depth the impact of the nature of the chemistry on the cohesive properties of polymer:fullerene or small-molecule:fullerene mixtures.

Importantly, we find that relatively modest changes in chemistry—i.e., the differences in substituent chemistry between PCBM and ICMA—can lead to rather important effects on the mechanical properties of the BHJ active layers. Seemingly marginal differences in the strength of intermolecular interactions among bulk fullerenes, in polymer:fullerene blends, and at polymer:fullerene interfaces, induced by the nature of the fullerene substituents, can result in different fracture processes taking place in BHJ active layers. Hence, an important message that arises from our study is that not only does fullerene substituent chemistry affect the miscibility and the morphology of the BHJ active layers that is known to be critical to the material electronic properties, it also affects the mechanical behavior of these films. Such considerations need to be taken into account for the robust manufacturing of OPV at industrial scales with high mechanical reliability.

ASSOCIATED CONTENT

Supporting Information

Schematic of four-point bend specimen and the layers of interest, elemental composition of fracture surfaces as measured by XPS, force field parameters used in the simulations, computed physical, mechanical, and surface properties, radial distribution function of PCBM and ICMA, fracture energy calculation for amorphous fullerene derivatives, density profiles for P3HT:fullerene derivative bilayers, average number of entanglements, discussion on entanglements in polymer:-nanoparticles mixtures. The Supporting Information is available free of charge on the ACS Publications website at DOI: 10.1021/acsami.5b02202.

AUTHOR INFORMATION

Corresponding Authors

*E-mail: dauskardt@stanford.edu (R.H.D.)
*E-mail: chad.risko@uky.edu (C.R.)
*E-mail: jean-luc.bredas@kaust.edu.sa (J.-L.B.).

Notes

The authors declare no competing financial interest.

ACKNOWLEDGMENTS

We gratefully acknowledge financial support of this work in part by the Center for Advanced Molecular Photovoltaics (CAMP, Award KUS-C1-015-21) made possible by King Abdullah University of Science and Technology (KAUST) and by the Office of Naval Research (Award No. N00014-14-1-0171). C.R. thanks the University of Kentucky Vice President for Research for start-up funds. Computing resources were provided through the National Science Foundation Chemistry Research Instrumentation and Facilities (CRIF) Program (Award No. CHE-0946869) and the Oklahoma Super Computing Center for Education and Research (OSCER). We are most grateful to Professor Martin Kröger (ETH Zürich) for the Z1 software package.

REFERENCES

(1) Brand, V.; Bruner, C.; Dauskardt, R. H. Cohesion and Device Reliability in Organic Bulk Heterojunction Photovoltaic Cells. *Sol. Energy Mater. Sol. Cells* **2012**, *99*, 182−189.
(2) Bruner, C.; Miller, N. C.; McGehee, M. D.; Dauskardt, R. H. Molecular Intercalation and Cohesion of Organic Bulk Heterojunction Photovoltaic Devices. *Adv. Funct. Mater.* **2013**, *23*, 2863−2871.
(3) Bruner, C.; Dauskardt, R. Role of Molecular Weight on the Mechanical Device Properties of Organic Polymer Solar Cells. *Macromolecules* **2014**, *47*, 1117−1121.
(4) Awartani, O.; Lemanski, B. I.; Ro, H. W.; Richter, L. J.; DeLongchamp, D. M.; O'Connor, B. T. Correlating Stiffness, Ductility, and Morphology of Polymer:Fullerene Films for Solar Cell Applications. *Adv. Energy Mater.* **2013**, *3*, 399−406.
(5) Anderson, T. L. *Fracture Mechanics: Fundamentals and Applications/T.L. Anderson*, 3rd ed.; Taylor & Francis: Boca Raton, FL, 2005.
(6) Liu, Y.; Gan, Q.; Baig, S.; Smela, E. Improving Adhesion of Polypyrrole to Gold for Long-Term Actuation, *Smart Structures and Materials 2005; Electroactive Polymer Actuators and Devices (EAPAD)*, San Diego, CA, USA; Bar-Cohen, Y., Ed.; 2005; pp 396−404.

DOI: 10.1021/acsami.5b02202
ACS Appl. Mater. Interfaces 2015, 7, 9957−9964

(7) Hauger, T. C.; Zeberoff, A.; Worfolk, B. J.; Elias, A. L.; Harris, K. D. Real-Time Resistance, Transmission and Figure-of-Merit Analysis for Transparent Conductors under Stretching-Mode Strain. *Sol. Energy Mater. Sol. Cells* **2014**, *124*, 247−255.
(8) Reese, M. O.; Morfa, A. J.; White, M. S.; Kopidakis, N.; Shaheen, S. E.; Rumbles, G.; Ginley, D. S. Pathways for the Degradation of Organic Photovoltaic P3ht:Pcbm Based Devices. *Sol. Energy Mater. Sol. Cells* **2008**, *92*, 746−752.
(9) Savagatrup, S.; Printz, A. D.; O'Connor, T. F.; Zaretski, A. V.; Rodriquez, D.; Sawyer, E. J.; Rajan, K. M.; Acosta, R. I.; Root, S. E.; Lipomi, D. J. Mechanical Degradation and Stability of Organic Solar Cells: Molecular and Microstructural Determinants. *Energy Environ. Sci.* **2015**, *8*, 55−80.
(10) Mikos, A. G.; Peppas, N. A. Polymer Chain Entanglements and Brittle Fracture. *J. Chem. Phys.* **1988**, *88*, 1337−1342.
(11) Williams, J. G. Fracture Mechanics of Polymers. *Polym. Eng. Sci.* **1977**, *17*, 144−149.
(12) Facchetti, A. Π-Conjugated Polymers for Organic Electronics and Photovoltaic Cell Applications. *Chem. Mater.* **2010**, *23*, 733−758.
(13) Mishra, A.; Bäuerle, P. Small Molecule Organic Semiconductors on the Move: Promises for Future Solar Energy Technology. *Angew. Chem., Int. Ed.* **2012**, *51*, 2020−2067.
(14) Kippelen, B.; Bredas, J. L. Organic Photovoltaics. *Energy Environ. Sci.* **2009**, *2*, 251−261.
(15) Bredas, J. L.; Durrant, J. R. Organic Photovoltaics. *Acc. Chem. Res.* **2009**, *42*, 1689−1690.
(16) Thompson, B. C.; Fréchet, J. M. J. Polymer−Fullerene Composite Solar Cells. *Angew. Chem., Int. Ed.* **2008**, *47*, 58−77.
(17) Liu, T.; Troisi, A. Absolute Rate of Charge Separation and Recombination in a Molecular Model of the P3ht/Pcbm Interface. *J. Phys. Chem. C* **2011**, *115*, 2406−2415.
(18) Idé, J.; Mothy, S.; Savoyant, A.; Fritsch, A.; Aurel, P.; Méreau, R.; Ducasse, L.; Cornil, J.; Beljonne, D.; Castet, F. Interfacial Dipole and Band Bending in Model Pentacene/C60 Heterojunctions. *Int. J. Quantum Chem.* **2013**, *113*, 580−584.
(19) Fu, Y.-T.; da Silva Filho, D. A.; Sini, G.; Asiri, A. M.; Aziz, S. G.; Risko, C.; Brédas, J.-L. Structure and Disorder in Squaraine−C60 Organic Solar Cells: A Theoretical Description of Molecular Packing and Electronic Coupling at the Donor−Acceptor Interface. *Adv. Funct. Mater.* **2014**, *24*, 3790−3798.
(20) Chen, W.; et al. Hierarchical Nanomorphologies Promote Exciton Dissociation in Polymer/Fullerene Bulk Heterojunction Solar Cells. *Nano Lett.* **2011**, *11*, 3707−3713.
(21) Rivnay, J.; Mannsfeld, S. C. B.; Miller, C. E.; Salleo, A.; Toney, M. F. Quantitative Determination of Organic Semiconductor Microstructure from the Molecular to Device Scale. *Chem. Rev.* **2012**, *112*, 5488−5519.
(22) Collins, B. A.; Li, Z.; Tumbleston, J. R.; Gann, E.; McNeill, C. R.; Ade, H. Absolute Measurement of Domain Composition and Nanoscale Size Distribution Explains Performance in PTB7:PC71BM Solar Cells. *Adv. Energy Mater.* **2013**, *3*, 65−74.
(23) Williams, M.; Tummala, N. R.; Aziz, S. G.; Risko, C.; Brédas, J.-L. Influence of Molecular Shape on Solid-State Packing in Disordered PC61BM and PC71BM Fullerenes. *J. Phys. Chem. Lett.* **2014**, 3427−3433.
(24) Tummala, N. R.; Mehraeen, S.; Fu, Y. T.; Risko, C.; Bredas, J. L. Materials-Scale Implications of Solvent and Temperature on [6,6]-Phenyl-C61-Butyric Acid Methyl Ester (PCBM): A Theoretical Perspective. *Adv. Funct. Mater.* **2013**, *23*, 5800−5813.
(25) Torabi, S.; et al. Strategy for Enhancing the Dielectric Constant of Organic Semiconductors without Sacrificing Charge Carrier Mobility and Solubility. *Adv. Funct. Mater.* **2015**, *25*, 150−157.
(26) He, Y.; Li, Y. Fullerene Derivative Acceptors for High Performance Polymer Solar Cells. *Phys. Chem. Chem. Phys.* **2011**, *13*, 1970−1983.
(27) Dai, L.; Mau, A. W. H. Controlled Synthesis and Modification of Carbon Nanotubes and C60: Carbon Nanostructures for Advanced Polymeric Composite Materials. *Adv. Mater.* **2001**, *13*, 899−913.
(28) Saotome, T.; Kokubo, K.; Shirakawa, S.; Oshima, T.; Hahn, H. T. Polymer Nanocomposites Reinforced with C60 Fullerene: Effect of Hydroxylation. *J. Compos. Mater.* **2011**, *45*, 2595−2601.
(29) Balta Calleja, F. J.; Giri, L.; Asano, T.; Mieno, T.; Sakurai, A.; Ohnuma, M.; Sawatari, C. Structure and Mechanical Properties of Polyethylene-Fullerene Composites. *J. Mater. Sci.* **1996**, *31*, 5153−5157.
(30) Knauert, S. T.; Douglas, J. F.; Starr, F. W. The Effect of Nanoparticle Shape on Polymer-Nanocomposite Rheology and Tensile Strength. *J. Polym. Sci., Part B: Polym. Phys.* **2007**, *45*, 1882−1897.
(31) Tuteja, A.; Duxbury, P. M.; Mackay, M. E. Multifunctional Nanocomposites with Reduced Viscosity. *Macromolecules* **2007**, *40*, 9427−9434.
(32) Fu, S.-Y.; Feng, X.-Q.; Lauke, B.; Mai, Y.-W. Effects of Particle Size, Particle/Matrix Interface Adhesion and Particle Loading on Mechanical Properties of Particulate−Polymer Composites. *Composites, Part B* **2008**, *39*, 933−961.
(33) Dupont, S. R.; Oliver, M.; Krebs, F. C.; Dauskardt, R. H. Interlayer Adhesion in Roll-to-Roll Processed Flexible Inverted Polymer Solar Cells. *Sol. Energy Mater. Sol. Cells* **2012**, *97*, 171−175.
(34) O'Connor, B.; Chan, E. P.; Chan, C.; Conrad, B. R.; Richter, L. J.; Kline, R. J.; Heeney, M.; McCulloch, I.; Soles, C. L.; DeLongchamp, D. M. Correlations between Mechanical and Electrical Properties of Polythiophenes. *ACS Nano* **2010**, *4*, 7538−7544.
(35) Steve, P. Fast Parallel Algorithms for Short-Range Molecular Dynamics. *J. Comput. Phys.* **1995**, *117*, 1−19.
(36) Berendsen, H. J. C.; Vanderspoel, D.; Vandrunen, R. Gromacs - a Message Passing-Parallel Molecular-Dynamics Implementation. *Comput. Phys. Commun.* **1995**, *91*, 43−56.
(37) Hess, B.; Kutzner, C.; van der Spoel, D.; Lindahl, E. Gromacs 4: Algorithms for Highly Efficient, Load-Balanced, and Scalable Molecular Simulation. *J. Chem. Theory Comput.* **2008**, *4*, 435−447.
(38) Parrinello, M.; Rahman, A. Polymorphic Transitions in Single Crystals: A New Molecular Dynamics Method. *J. Appl. Phys.* **1981**, *52*, 7182−7190.
(39) Nose, S. A Unified Formulation of the Constant Temperature Molecular Dynamics Methods. *J. Chem. Phys.* **1984**, *81*, 511−519.
(40) Tuckerman, M. E.; Alejandre, J.; López-Rendón, R.; Jochim, A. L.; Martyna, G. J. A Liouville-Operator Derived Measure-Preserving Integrator for Molecular Dynamics Simulations in the Isothermal−Isobaric Ensemble. *J. Phys. A: Math. Gen.* **2006**, *39*, 5629.
(41) Jorgensen, W. L.; McDonald, N. A. Development of an All-Atom Force Field for Heterocycles. Properties of Liquid Pyridine and Diazenes. *J. Mol. Struct.: THEOCHEM* **1998**, *424*, 145−155.
(42) Frigerio, F.; Casalegno, M.; Carbonera, C.; Nicolini, T.; Meille, S. V.; Raos, G. Molecular Dynamics Simulations of the Solvent- and Thermal History-Dependent Structure of the Pcbm Fullerene Derivative. *J. Mater. Chem.* **2012**, *22*, 5434−5443.
(43) Cheung, D. L.; Troisi, A. Theoretical Study of the Organic Photovoltaic Electron Acceptor PCBM: Morphology, Electronic Structure, and Charge Localization†. *J. Phys. Chem. C* **2010**, *114*, 20479−20488.
(44) Do, K.; Huang, D. M.; Faller, R.; Moule, A. J. A Comparative Md Study of the Local Structure of Polymer Semiconductors P3HT and PBTTT. *Phys. Chem. Chem. Phys.* **2010**, *12*, 14735−14739.
(45) Schwarz, K. N.; Kee, T. W.; Huang, D. M. Coarse-Grained Simulations of the Solution-Phase Self-Assembly of Poly(3-Hexylthiophene) Nanostructures. *Nanoscale* **2013**, *5*, 2017−2027.
(46) Tummala, N. R.; Risko, C.; Bruner, C.; Dauskardt, R. H.; Brédas, J.-L. Entanglements in P3HT and Their Influence on Thin-Film Mechanical Properties: Insights from Molecular Dynamics Simulations. *J. Polym. Sci., Part B: Polym. Phys.* **2015**, DOI: 10.1002/polb.23722.
(47) Tuckerman, M. E.; Mundy, C. J.; Balasubramanian, S.; Klein, M. L. Modified Nonequilibrium Molecular Dynamics for Fluid Flows with Energy Conservation. *J. Chem. Phys.* **1997**, *106*, 5615−5621.
(48) Foteinopoulou, K.; Karayiannis, N. C.; Mavrantzas, V. G.; Kröger, M. Primitive Path Identification and Entanglement Statistics in

DOI: 10.1021/acsami.5b02202
ACS Appl. Mater. Interfaces 2015, 7, 9957−9964

Polymer Melts: Results from Direct Topological Analysis on Atomistic Polyethylene Models. *Macromolecules* **2006**, *39*, 4207−4216.
(49) Shanbhag, S.; Kröger, M. Primitive Path Networks Generated by Annealing and Geometrical Methods: Insights into Differences. *Macromolecules* **2007**, *40*, 2897−2903.
(50) Karayiannis, N. C.; Kröger, M. Combined Molecular Algorithms for the Generation, Equilibration and Topological Analysis of Entangled Polymers: Methodology and Performance. *Int. J. Mol. Sci.* **2009**, *10*, 5054−5089.
(51) Hoy, R. S.; Foteinopoulou, K.; Kröger, M. Topological Analysis of Polymeric Melts: Chain-Length Effects and Fast-Converging Estimators for Entanglement Length. *Phys. Rev. E: Stat. Phys., Plasmas, Fluids* **2009**, *80*, 031803.
(52) Machui, F.; Abbott, S.; Waller, D.; Koppe, M.; Brabec, C. J. Determination of Solubility Parameters for Organic Semiconductor Formulations. *Macromol. Chem. Phys.* **2011**, *212*, 2159−2165.
(53) Machui, F.; Langner, S.; Zhu, X.; Abbott, S.; Brabec, C. J. Determination of the P3HT:PCBM Solubility Parameters Via a Binary Solvent Gradient Method: Impact of Solubility on the Photovoltaic Performance. *Sol. Energy Mater. Sol. Cells* **2012**, *100*, 138−146.
(54) Hansen, C. M. "The Three Dimensional Solubility Parameter-Key to Paint Component Affnitiies": I. Solvents, Plasticizers, Polymers and Resins. *J. Paint Technol.* **1967**, *39*, 104.
(55) The Hildebrand parameter (δ_T) is defined as the square-root of the cohesive energy density (CED), where the CED is the intermolecular interaction energy in solid phase per unit volume. Hansen further separated the Hildebrand parameter into three intermolecular contributions: dispersive (δ_D), Coulombic or dipole−dipole (δ_P), and hydrogen-bonding (δ_H) interactions, respectively.
(56) Duong, D. T.; Walker, B.; Lin, J.; Kim, C.; Love, J.; Purushothaman, B.; Anthony, J. E.; Nguyen, T.-Q. Molecular Solubility and Hansen Solubility Parameters for the Analysis of Phase Separation in Bulk Heterojunctions. *J. Polym. Sci., Part B: Polym. Phys.* **2012**, *50*, 1405−1413.
(57) Chen, D.; Nakahara, A.; Wei, D.; Nordlund, D.; Russell, T. P. P3HT/PCBM Bulk Heterojunction Organic Photovoltaics: Correlating Efficiency and Morphology. *Nano Lett.* **2010**, *11*, 561−567.
(58) Lin, Y.-H.; Tsai, Y.-T.; Wu, C.-C.; Tsai, C.-H.; Chiang, C.-H.; Hsu, H.-F.; Lee, J.-J.; Cheng, C.-Y. Comparative Study of Spectral and Morphological Properties of Blends of P3HT with PCBM and ICMA. *Org. Electron.* **2012**, *13*, 2333−2341.
(59) Hoen, S.; Chopra, N. G.; Xiang, X. D.; Mostovoy, R.; Hou, J.; Vareka, W. A.; Zettl, A. Elastic Properties of a Van Der Waals Solid: C60. *Phys. Rev. B: Condens. Matter* **1992**, *46*, 12737−12739.
(60) Kolomenskii, A. A.; Szabadi, M.; Hess, P. Laser Diagnostics of C60 and C70 Films by Broadband Surface Acoustic Wave Spectroscopy. *Appl. Surf. Sci.* **1995**, *86*, 591−596.
(61) Kobelev, N. P.; Nikolaev, R. K.; Soifer, Y. M.; Khasanov, S. S. Elastic Moduli of Single-Crystal C60. *Phys. Solid State* **1998**, *40*, 154−156.
(62) Zhao, Q.; Wood, J. R.; Wagner, H. D. Stress Fields around Defects and Fibers in a Polymer Using Carbon Nanotubes as Sensors. *Appl. Phys. Lett.* **2001**, *78*, 1748−1750.
(63) Gumbsch, P.; Cannon, R. M. Atomistic Aspects of Brittle Fracture. *MRS Bull.* **2000**, *25*, 15−20.
(64) Huang, J. H.; Hsiao, Y. S.; Richard, E.; Chen, C. C.; Chen, P. L.; Li, G.; Chu, C. W.; Yang, Y. The Investigation of Donor-Acceptor Compatibility in Bulk-Heterojunction Polymer Systems. *Appl. Phys. Lett.* **2013**, *103*, 043304.
(65) Nilsson, S.; Bernasik, A.; Budkowski, A.; Moons, E. Morphology and Phase Segregation of Spin-Casted Films of Polyfluorene/Pcbm Blends. *Macromolecules* **2007**, *40*, 8291−8301.
(66) Wang, Y.; Alcamí, M.; Martín, F. Understanding the Supramolecular Self-Assembly of the Fullerene Derivative Pcbm on Gold Surfaces. *ChemPhysChem* **2008**, *9*, 1030−1035.
(67) Rottler, J.; Barsky, S.; Robbins, M. O. Cracks and Crazes: On Calculating the Macroscopic Fracture Energy of Glassy Polymers from Molecular Simulations. *Phys. Rev. Lett.* **2002**, *89*, 148304.
(68) Tahk, D.; Lee, H. H.; Khang, D.-Y. Elastic Moduli of Organic Electronic Materials by the Buckling Method. *Macromolecules* **2009**, *42*, 7079−7083.
(69) Baljon, A. R. C.; Robbins, M. O. Simulations of Crazing in Polymer Glasses: Effect of Chain Length and Surface Tension. *Macromolecules* **2001**, *34*, 4200−4209.
(70) Kausch, H. H.; Devries, K. L. Molecular Aspects of High Polymer Fracture as Investigated by Esr-Technique. *Int. J. Fract.* **1975**, *11*, 727−759.

DOI: 10.1021/acsami.5b02202
ACS Appl. Mater. Interfaces 2015, 7, 9957−9964